# CHAPTER 2 REVIEW AND THEORY

This chapter remarks the introduction to DLC, metastable form of amorphous carbon and mechanical properties of DLC films, the related theories, documents, and research topics which are related to thin film various deposition technique, especially by filtered cathodic arc method, DLC deposition mechanism, DLC/a-Si thin film deposition by pulse filtered cathodic arc method and characterization of DLC/a-Si thin films.

## 2.1 Diamond-Like Carbon

### 2.1.1 Introduction

DLC (diamond-like carbon) is a metastable form of amorphous carbon containing a significant fraction of $sp^3$ bonds. It can have a high mechanical hardness, optical transparency, chemical inertness, and it is a wide band gap semiconductor [14-17]. It is widespread application used as protective coating in areas such as car parts, optical windows, biomedical devices, magnetic recording heads, and as micro electro mechanical devices (MEMs).

The carbon forms a great variety of crystalline and disordered structures because it is able to exist in three hybridization, $sp^3$, $sp^2$ and $sp^1$ configurations as shown in Figure 2.1.

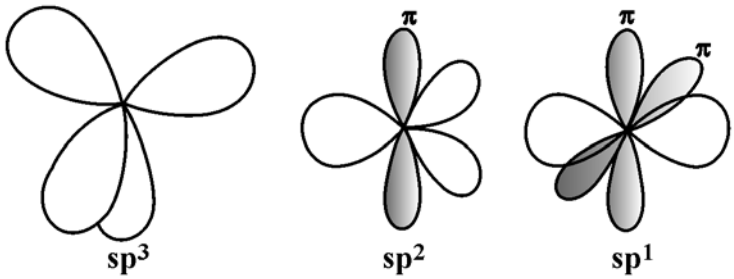


**Figure 2.1** sp3, $sp^2$ and $sp^1$ configurations.

### 2.1.2 Bonding

**Atomic orbital**

Orbital is a probability function to find electron in a certain space. It also often called the electron density, Carbon's atomic orbital are two types call s and p orbital the shape as shown in Figure 2.2.

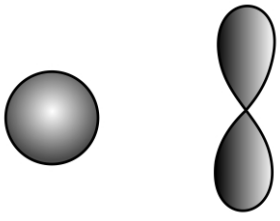

**Figure 2.2** Shape of 1s and 2p orbitals.

**Sigma "σ" and Pi Bonds "π"**

A Sigma bond "σ" is the strongest chemical covalent bond. It is created by the "end-to-end" overlap of atomic orbitals. Going more in depth, it is in which the region of electron sharing is along the imaginary line which connects the bonded atoms. They can be formed from two s-orbitals, two p-orbitals, one s- and p- orbital, or with sp hybrid orbitals as shown in Figure 2.3.

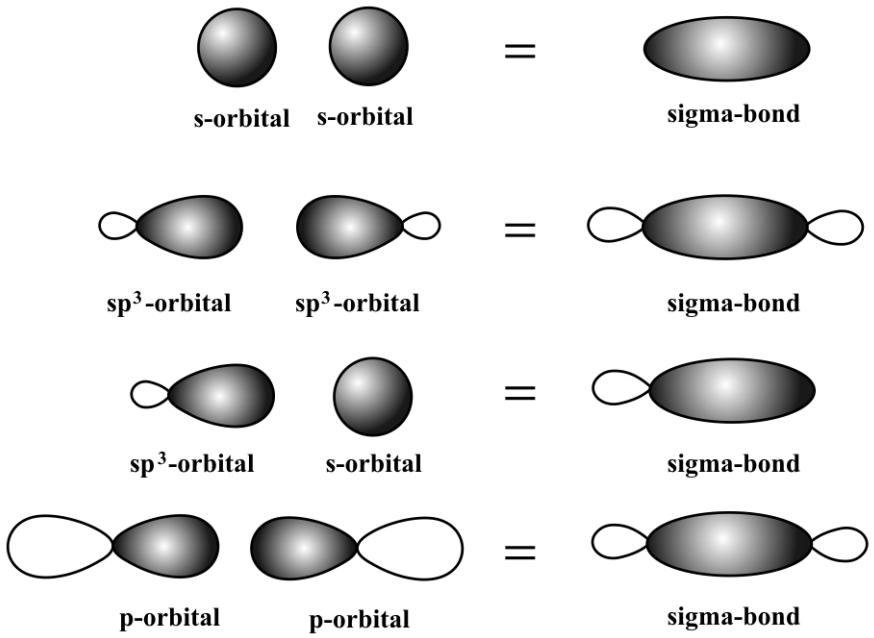


**Figure 2.3** Sigma bond created from two s atomic orbitals.

Pi Bonds "π" are created by the "side-to-side" overlapping of two parallel p-orbitals as shown in Figure 2.4. A pi bond is a weaker chemical covalent bond than a sigma bond (since π bonds have a smaller overlap between the orbitals).

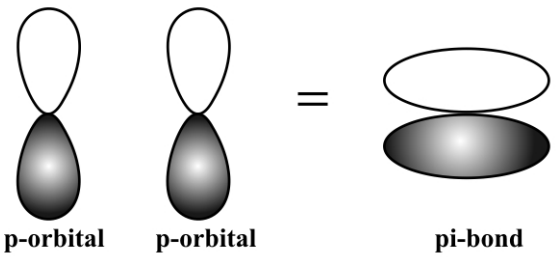


**Figure 2.4** Two p-orbitals in the first diagram overlap to create pi bonds.

## 2.1.3 Hybridization

Hybridization is the concept of mixing atomic orbitals to form new *hybrid orbitals* suitable for the qualitative description of atomic bonding properties.

**$sp^3$ hybridization**

In organic chemistry hybridization of carbon is most important. Carbon has four electrons in the outer most valence shell. The energy level of these electrons in ground state and hybridized state of carbon atom (Figure 2.5) $sp^3$ hybridized orbital are formed by promoting one '2S' electron to vacant 'P' orbital and mixing all four orbital to form four hybrid orbital of equal energy, capable of forming four σ bonds. The shaped formed is tetrahedral with each electron at each corner as shown in Figure 2.6

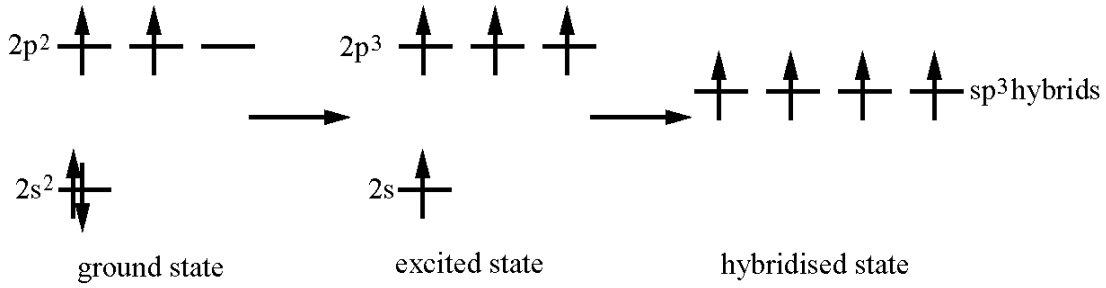


**Figure 2.5** $sp^3$ hybridization mechanism [18].

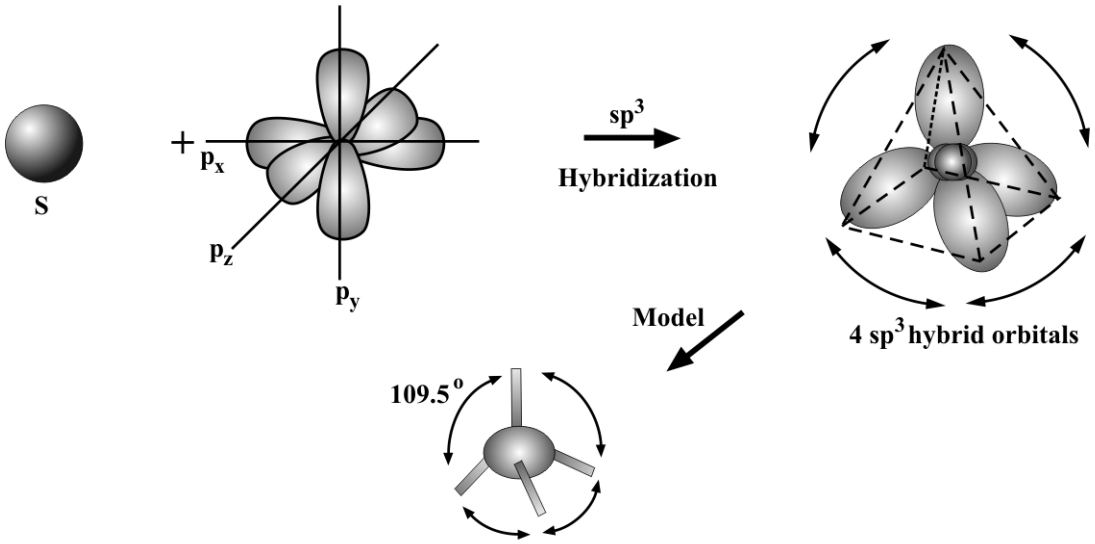


**Figure 2.6** $sp^3$ configuration.

**$sp^2$ hybridization**

When a C atom is attached to 3 groups and so is involved in 3 σ bonds, it requires 3 orbitals in the hybrid set. This requires that it is $sp^2$ hybridised. The general "steps" are similar to that for seen previously $sp^3$ hybridization and $sp^2$ hybridization mechanisms as shown in Figure 2.7. And the shaped of $sp^2$ (Figure 2.8).

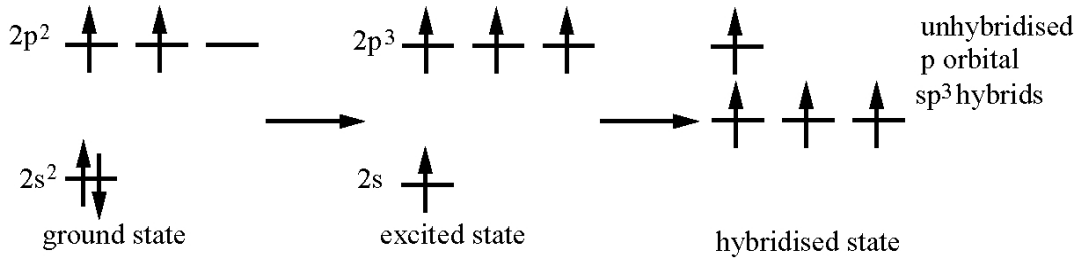


**Figure 2.7** $sp^2$ hybridization mechanism [18].

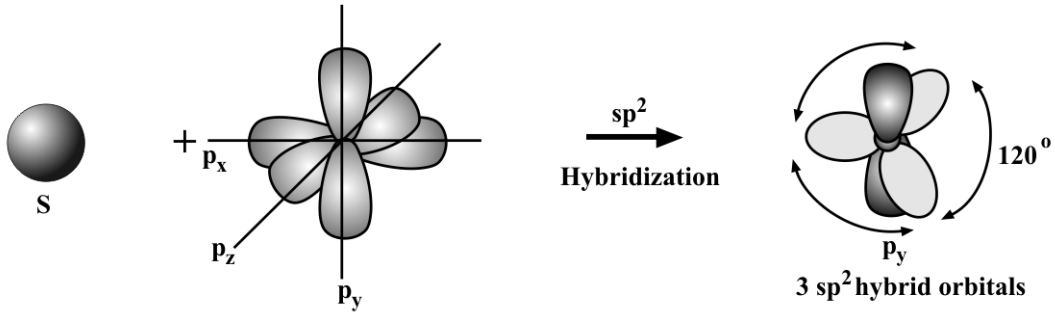


**Figure 2.8** $sp^2$ configuration.

**sp hybridization**

When a C atom is attached to 2 groups and so is involved in 2 σ bonds, it requires 2 orbitals in the hybrid set. This requires that it is sp hybridised. The general "steps" are similar to that for seen previously $sp^3$ and $sp^2$ hybridization. The sp hybridization mechanisms shown in Figure 2.9. And the shaped of sp (Figure 2.10).

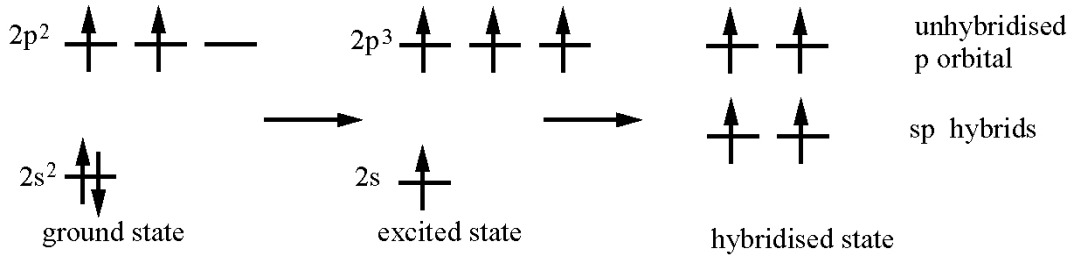


**Figure 2.9** sp hybridization mechanism [18].

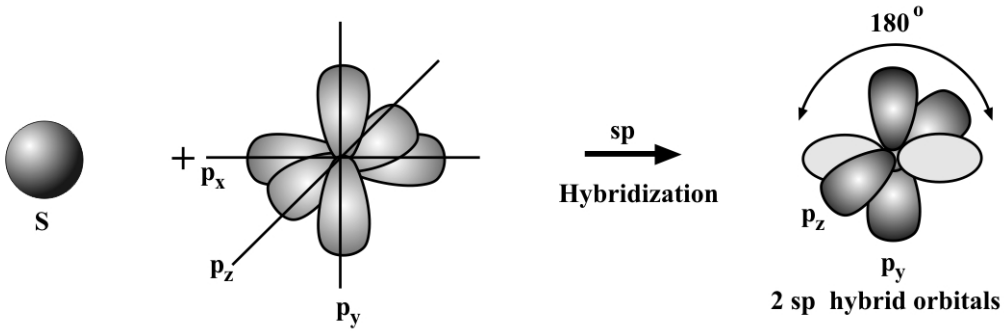


**Figure 2.10** $sp^1$ configuration.

In the $sp^3$ configuration, as in diamond, a carbon atom's four valence electrons are each assigned to a tetrahedrally directed $sp^3$ orbital (ta-C), as in diamond lattice. Which makes a strong σ bond to an adjacent atom that is strongest type of covalent chemical bond. The $sp^2$, in the three-fold coordinated $sp^2$ configuration as in graphite, three of the four valence electrons enter a trigonally directed $sp^2$ orbitals, which form σ bond in a plane. The fourth electron of the $sp^2$ atom lies in pπ orbital, which lies normal to the σ bonding plane. This π orbital forms a weaker π bond with an π orbital on one or more neighboring atoms. The $sp^1$ configuration, two of four valence electrons enter σ orbital, each forming a σ bond directed along ±x axis, and the other two electrons enter pπ orbital in y and z direction.

DLC has some extreme properties similar to diamond, such as chemical inertness, elastic modulus, hardness, but these are achieved in an isotropic disordered thin film with no grain boundaries. It is cheaper to produce than diamond itself. This has powerfully advantage for much application. Various deposition techniques have been developed to synthesize amorphous carbon with purpose to increase $sp^3$ fraction. Amorphous carbon with high $sp^3$ fraction will be called tetrahedral amorphous carbon (ta-C) while hydrogenated tetrahedral amorphous carbon (ta-C:H) was introduced by Weiler, et al. [19]. for a hydrogen containing carbon film. Typical properties of the various forms of DLC are compared to diamond and graphite in Table 2.1 [19-25].

**Table 2.1** Typical properties of amorphous carbon, diamond, graphite, $C_{60}$ and polyethylene.

| | $sp^3$ (%) | H (%) | Density (g $cm^{-3}$) | Gap (eV) | Hardness (GPa) |
|---|---|---|---|---|---|
| Diamond | 100 | 0 | 3.515 | 55 | 100 |
| Graphite | 0 | 0 | 2.267 | 0 | |
| $C_{60}$ | 0 | 0 | | 1.6 | |
| Glassy C | 0 | 0 | 1.3-1.55 | 0.01 | 3 |
| Evaporated C | 0 | 0 | 1.9 | 0.4-0.7 | 3 |
| Sputtered C | 5 | 0 | 2.2 | 0.5 | |
| ta-C | 80-88 | 0 | 3.1 | 2.5 | 80 |
| a-C:H hard | 40 | 30-40 | 1.6-2.2 | 1.1-1.7 | 10-20 |
| a-C:H Soft | 60 | 40-50 | 1.2-1.6 | 1.7-4 | <10 |
| ta-C:H | 70 | 30 | 2.4 | 2.0-2.5 | 50 |
| Polyethylene | 100 | 67 | 0.92 | 6 | 0.01 |

The $sp^3$ bonding of DLC confers on it many of the beneficial properties of diamond itself, such as its chemical and electrochemical inertness, mechanical hardness, and wide band gap. DLC consist of the amorphous carbon (a-C), the hydrogenated alloys and a-C:H. It is comfortable to exhibit the composition of the various forms of amorphous C-H alloys on a ternary phase diagram as shown in Figure 2.11, as obtained by Jacob and Moller [25]. There are many a-Cs with disordered graphitic ordering, such as glassy carbon, chars, soot, and evaporated a-C. These lie in the lower left hand corner. The two hydrocarbon polymers polyethylene $(CH_2)_n$ and polyacetylene $(CH)_n$ define the limits of a triangle in the right hand corner beyond which interconnecting C-C networks cannot form, and only molecules form.

The ternary phase diagram, first used by Jacob and Moller [25], is a chart to show a various form of amorphous C-H, as in Figure 2.11. The lower left hand corner show disordered graphite ordering, such as glassy carbon, evaporated a-C. The right hand side shows hydrocarbon polymer and limitation in a triangle that C-C cannot forms.

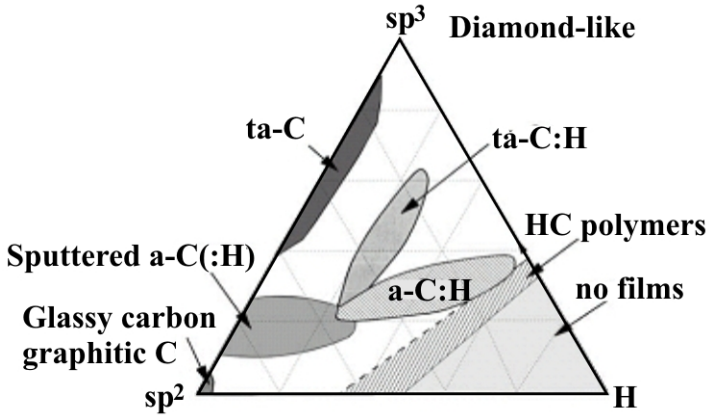


**Figure 2.11** Ternary diagram, $sp^2$, $sp^3$ and H-Content of ta-C, ta-C: H, a-C:H and a-C [25].

## 2.2 Diamond-Like Character

The 'diamond–like' character of DLC films obviously arises from its carbon $sp^3$ bonds. The DLC is amorphous phase and atomically. It is a random network. The mechanical properties of this network can be considered as the alloy of difference bonding components, $sp^3$, $sp^2$, $sp^1$and C-H bonds. The Young's modulus, hardness and diamond-like quality arise from the $sp^3$ bonds. The $sp^2$ and $sp^1$ doesn't contribution much. The C-H bonds don't like up the network, they are just like a dangling bonds and not contribution to mechanical properties. The Young's modulus was depending on the $sp^3$ fraction, also the density of a-C varies linearly on the $sp^3$ fraction.

Figure 2.12 shows the $sp^3$ fraction varies for ta-C deposited by FCA [21, 26]. The maximum $sp^3$ fraction is around 100eV, the increasing $sp^3$ fraction at low ion energy is controlled by penetration probability and the decline in $sp^3$ fraction at high ion energy is controlled by the relaxation of C ion in subsurface.

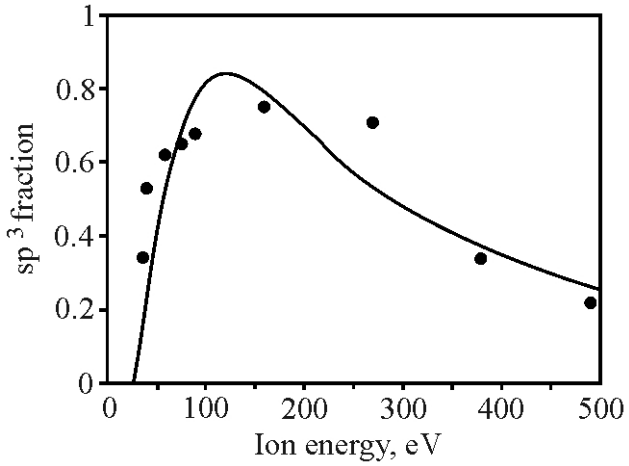


**Figure 2.12** Comparison of calculated C-C $sp^3$ fraction of ta-C, with experimental data of Fallon, et al. [21].

## 2.3 Deposition Method for DLC

### 2.3.1 Ion Beam Deposition

The first DLC were prepared as thin films by Aisenberg and Chabot [27] using ion beam deposition. The common feature of these DLC deposition methods is condensed from a beam containing medium energy (~100 eV) carbon or hydrocarbon ions. There are two processes involved for this method to DLC film growth, a physical process due to the impact of ions on the growing film helps formation of $sp^3$ bonding. This contrasts with the chemical vapor deposition (CVD) of diamond, where a chemical process stabilizes its $sp^3$ bonding [28]. A typical ion beam deposition system, the plasma sputtering of graphite cathode in an ion source which produce carbon ions [27, 29-32]. The filament dc discharge ion source such as. Kaufman gun was the first ion beam DLC system. However, the RF ICP ion source has since been developed for direct ion beam deposition of DLC films with benefit in longer mean time between maintenance (MTBM) and reliability to control energy of ions. RF ICP source principle that is design by Veeco Instruments Inc is described following;

The quartz discharge vessel is the ion source chamber wrapped with a helical RF coil to generate sinusoidal Radio Frequency (RF) magnetic field. The induced electrical field created inside vessel produce accelerated electrons ionizes and neutral gas molecule. The operating frequency of 1.8 MHz is normally used to minimize internal sputtering and capacitive coupling. Hydrocarbon gas such as methane is purge into quartz chamber at one end, plasma beam generated by RF is extracted at the other end by ion optics consisting of three planar grids. The inner plate is called beam grid, is supplied with positive potential. The middle plate is held at negative potential, and is called suppressor. The outer plate which is not biased is called a ground plate. The PBN (plasma bridge neutralizer) is electron source used to ignite plasma and neutralize charges as schematically in Figure 2.13.

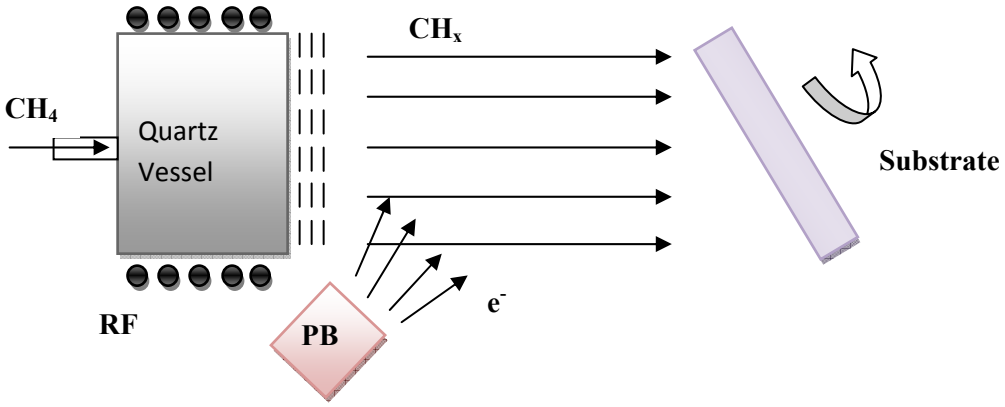


**Figure 2.13** Schematic of RF ICP ion beam source.

### 2.3.2 Mass Selected Ion Beam

The mass selected ion beam deposition (MSIB) method were controlled the desirable a single ion species at a well-defined ion energy as same as the name MSIB. Carbon ions are produced in an ion source from a graphite target, such that the spread of ion energies is small, 1-10 V. The ions are then accelerated to 5-40 kV and passed thought a magnetic filter. This filters out any neutrals and selects ions with an e/m ration of the $C^+$ ion. The ions beam will diverge because of its coulombic repulsion. Their ions are then decelerated to the desired ion energy by electrostatic lens, thereafter the beam is focus onto substrate in a vacuum of order $10^{-8}$ Torr to produce ta-C films.

### 2.3.3 Chemical Vapor Deposition (CVD)

The CVD process is chemical reactions such as methane or ethylene is used as hydrocarbon gas. The key parameter that influencing the reaction are the gas flow, gas composition and the temperature.

There are several CVD processes that are widely spread used for DLC growth [33]. Such as using tungsten hot filament activation a simply thermal process that generate heated up to 1900-2500 °C which a high deposition rate. Plasma activation using frequency power source which is available in commercial such as13.56 MHz, 915MHz and 2.45 GHz for the synthesis. The advantage of plasma activation is substrate temperature is lower than the hot filament system due to a radical species can be created from high-energy electron.

The radio frequency inductively couple plasma source (ICPS) has been develop since 1990s. The system provides a high-density with low capacitive coupling, improves uniformity and operated in order of low-pressure. The study of RF-ICPECVD was introduced by Yu, S.J. et al. [34] with schematic is shown in Figure 2.14. The system consists of single circular couple coil wrapped around chamber supplied with RF power to create induced electrical field inside chamber. Methane ($CH_4$) gas was used. The gas molecules were ionized by electrons accelerated using electric field to form inductive couple plasma. Bias supplied is also used in order to control bias voltage. The substrate temperature monitor by thermocouple was approximately 50 °C.

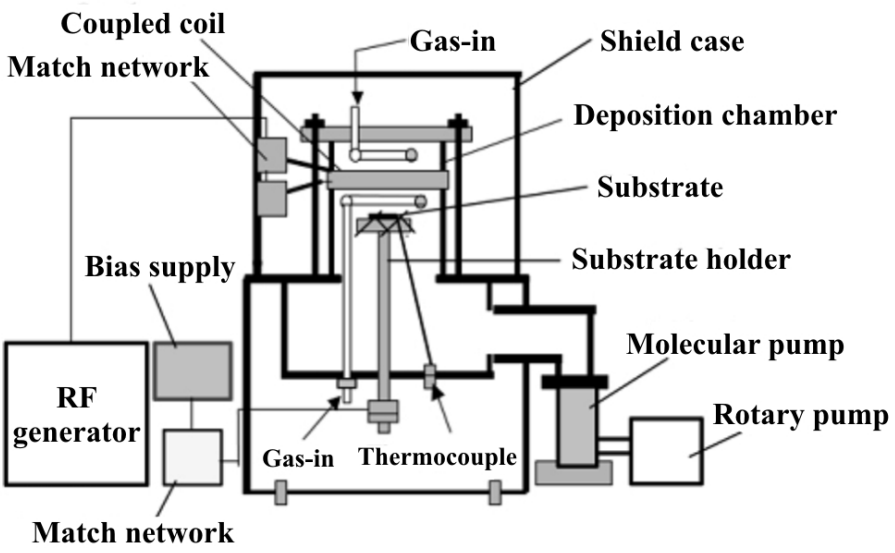


**Figure 2.14** Schematic diagram of RF-ICPECVD.

ECR (Electron Cyclotron Resonance) is plasma enhanced chemical vapor deposition (CVD) which separate plasma generation region from substrate like ion beam deposition that was purposed to reduce substrate temperature during process. The microwave frequency creates electron cyclotron resonance (ECR) effect. The schematic of ECR-CVD system is shown in Figure 2.15 (Kuramoto, K. et al.) [35].

The substrate is supplied with 13.56 MHz RF for self bias voltage control. Argon gas is normally introduced in ECR source while methane is applied near the substrate. Experiment show increasing of film hardness and deposition rate that are related to the increasing of bias voltage at substrate. The temperature at substrate is lower than 70 °C while produced DLC film is produced and a high deposition rate more than 80 nm/min is generally archived. The disadvantage is found with ultrathin DLC (<5nm) where deposition of films are too fast.

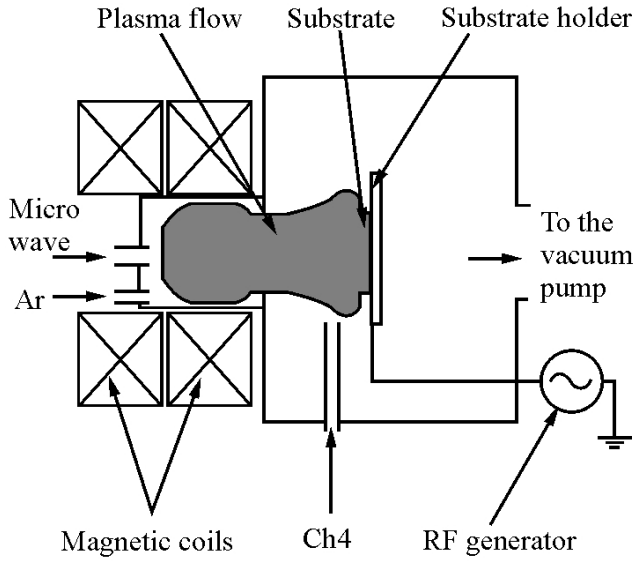


**Figure 2.15** Schematic of ECR-CVD system [35].

### 2.3.4 Plasma-Enhanced Chemical Vapor Deposition (PECVD)

The DLC coating is deposited by adsorption of most free radicals of hydrocarbon to the substrate and chemical bonding to the other atom on the surface. The hydrocarbon species are produce by the RF plasma decomposition of hydrocarbon precursors such as acetylene ($C_2H_2$) [36] at lower temperatures than those utilized in CVD reactors without settling for a lesser film quality, also results in a higher deposition rate and good step coverage, the energic in electrons in the plasma (at pressure ranging from 1 to 5 x $10^2$ Pa, typical less than 10 Pa) can activate almost any reaction among the gases in the glow discharge at relatively low substrate temperature ranging from 100 °C to 600 °C (typical less than 300 °C). To deposit the coating on non-silicon substrate, about 4 nm thick amorphous silicon adhesion layers, used to improve adhesion, is first deposited under similar conditions from a gas mixture of 1 % silane in argon. The schematic of PECVD system is shown in Figure 2.16.

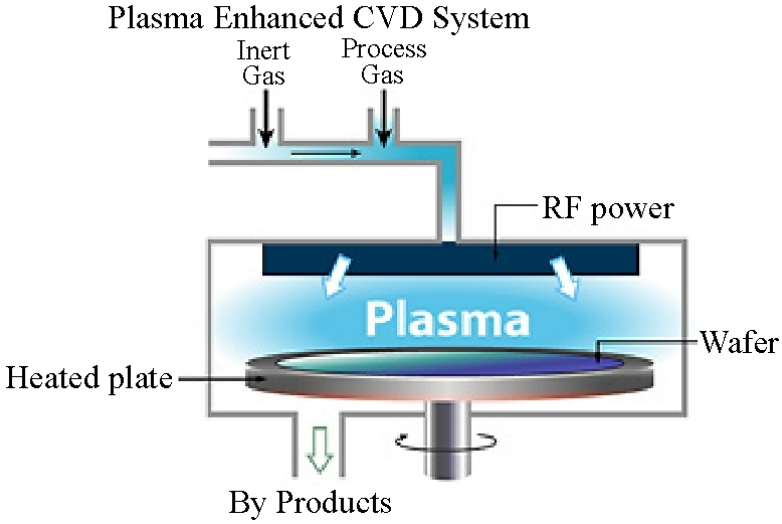


**Figure 2.16** Schematic of PECVD system.

### 2.3.5 Pulsed Laser Deposition

This deposition method use pulsed excimer laser to vaporize materials as an intense plasma [16, 37-43], for example ArF is give very short intense energy pulses. The plasma then expands towards the substrate which produce kinetic energy, from this expansion gives ion energy analogous to the ion energy of MSIB or the cathodic arc. The mean ion energy is proportional to the laser fluency concentration at the target spot. In this way pulse laser deposition produce ta-C film similar to produce using FCA and MSIB method.

### 2.3.6 Sputtering

The sputtering process for DLC uses DC or RF sputtering of graphite electrode by Ar plasma. As graphite has low sputter yield, thus the deposition rate enhancement is often archived by using magnetron sputtering by placed magnets behind the target to cause the electrons to spiral and increase their path length, thus to increase the degree of ionization of the plasma as shown schematically in Figure 2.17. As ion bombardment

assist the formation of $sp^3$ bonding, the magnetic field can be configured to pass across to the substrate, so this cause the Ar ions to also bombard the substrate, to give an 'unbalanced magnetron'. The substrate can be applied DC bias voltage for vary the ion energy. Using of argon with methane or hydrogen can produce a-C: H, also a-C: $N_x$ can be synthesized with plasma of argon-nitrogen.

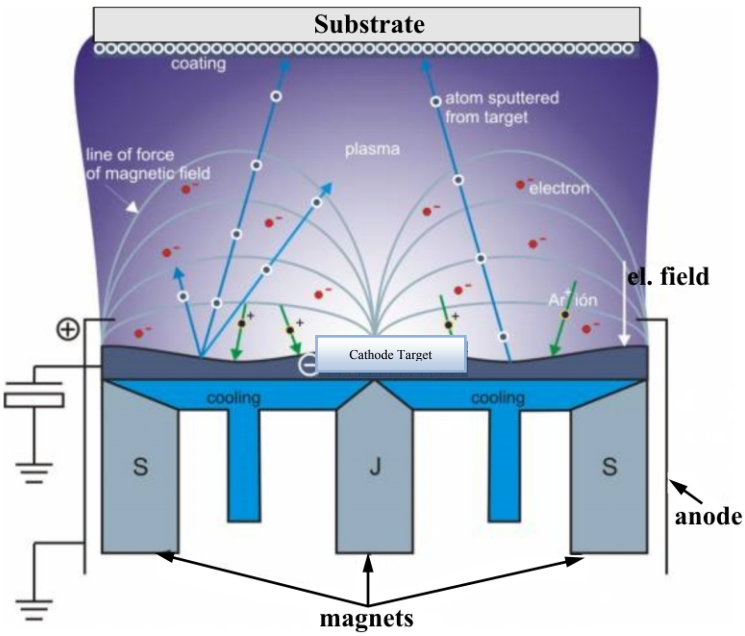


**Figure 2.17** DC magnetron sputtering system.

Alternatively, in the ion beam sputtering, Ar ions beam can be used to sputter graphite target to create the carbon flux [44]. A second Ar ion beam can be used to bombard the growing film, to densify the film or enhance $sp^3$ bonding. This is callion beam assisted deposition (IBD) or ion plating as shown schematically in Figure 2.18.

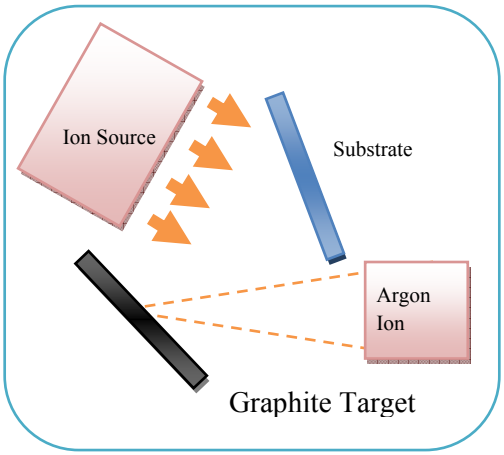


**Figure 2.18** Ion beam assisted deposition system.

### 2.3.7 Filtered Cathodic Arc

DLC deposition process using cathodic arc plasma produce an energetic plasma with a high ion density of up to $10^{13}$ $cm^3$. An igniter is used to ignite plasma or cathode spot that are two techniques, first is initiated in a high vacuum by touching the graphite cathode with a small carbon striker electrode and withdrawing the striker, and or high voltage between anode and cathode. A typical cathodic arc system as shown in Figure 2.19. The power supply is a high current with low voltage.

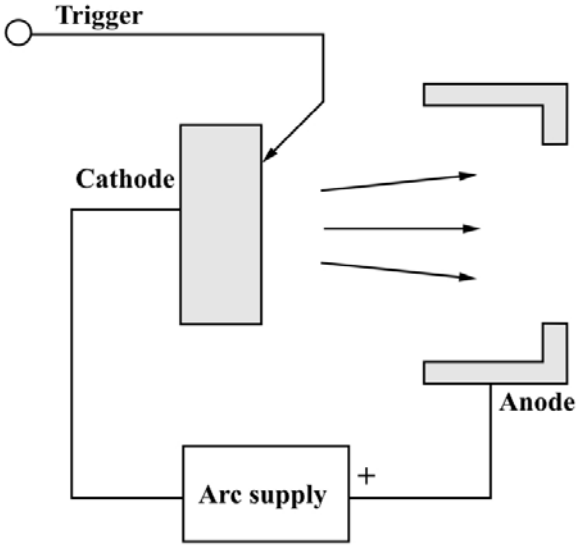


**Figure 2.19** Simplified schematic of basic cathodic arc configuration.

The cathode spot is small around 1-10 μm and it carries a very high current of density up to $10^6$–$10^8$ A $cm^{-2}$. The spot is created by an explosive emission process which generates the macro particles. The macro particle can be filtered by passing the plasma through a toroidal magnetic filter duct [45] as shown in Figure 2.20. The toroidal current for produce magnetic field around 0.1 Tesla along the axis of the filtered. The motion of electron of plasma spiral around the magnetic field line and follow along the filter axis. This motion produces an electrostatic field, which cause the positive ions to follow the electron around the filter. This produce an amipolar transport of plasma around the filter. The macro particle cannot follow the magnetic field and it hit the walls and baffles on the walls. Alternatively, in the open filter system used by Brown [45] and Anders, et al. [46], the macro particle and neutrals pass between the coil out of filter zone hit the wall in the chamber. Therefore, the filter raises the plasma ionization from about 30% to nearly 100% at the filter exit. The plasma beam is condensed onto a substrate to produce ta-C films. The plasma ion energies depending on the arc current. A DC or RF self-bias voltage can be applied to substrate for increase the incident ion energy [21]. The filter cathodic arc should be operated in pressure around $10^{-8}$ Torr, but sometime rise to $10^{-5}$ when plasma running. The arc can run in continuously or in pulse mode. The pulse mode operates by using a capacitor bank to strike the arc, or by laser initiation. The pulse mode is better in term of filtering due to ion tend to be entrained in plasma beam during the pulse while fall out of the plasma when beam stop [47].

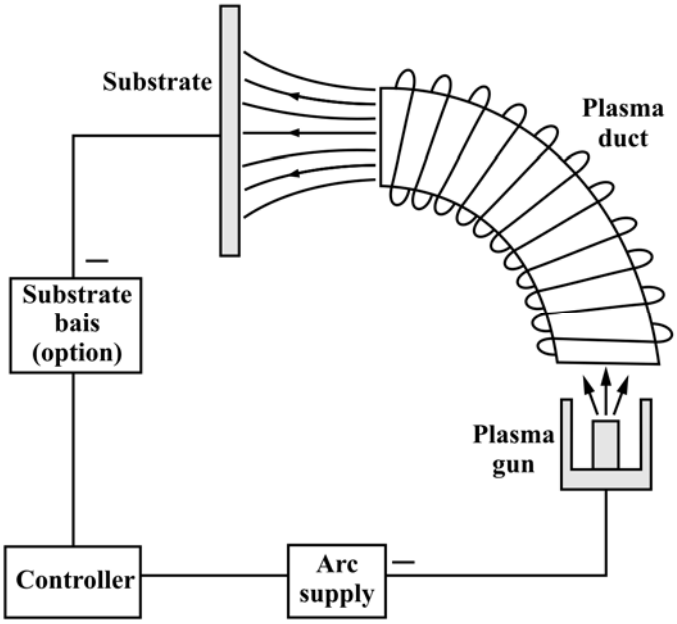


**Figure 2.20** Simplified schematic of basic magnetic filtered configuration.

## 2.4 DLC Property

### 2.4.1 Mechanical Property

The mechanical properties of DLCs are of great importance because of the use of DLC as a protective coating [48-51]. This properties are directly related to the fraction of $sp^3$ C–C bonds due to this bonding high bond energy per unit volume in all three directions of space. The ta-C films are being studied for possible use in MEMs instead of polysilicon. This is because ta-C is the hardest material known after diamond itself. A great advantage of DLC is amorphous with no grain boundaries, namely, the films are extremely smooth. DLC is also deposited at room temperature, which is an advantage for temperature sensitive substrate such as plastic. DLC also have extremely good coverage, so that they act as good corrosion barriers. This is particularly useful in major application, which is to coat disks and recording heads in the magnetic storage technology [50-51]. The disadvantage of DLC films are their intrinsic stress and thermal stability.

### 2.4.2 Adhesion

The majority of DLC is use for protective coating film. Therefore, thick films are preferred for this objective, to maximize wear life. The compressive stress limits the maximum thickness of adhesive films. A film of thickness h will delaminate when the elastic energy per unit volume due to the stress σ exceeds the surface fracture energy γ per surface, so for adhesion

$$2\gamma > \frac{\sigma^2 h}{2E} \tag{2.1}$$

or

$$h < \frac{4\gamma E}{\sigma^2} \qquad (2.2)$$

This set an upper limit of film thickness. The basic problem of DLC coatings was noted by Tamor [52]. The stress, Young's modulus and hardness all tend to be proportional to each other. When maximizing of the DLC film hardness means that the compressive stress is maximum also. Thus, maximizing of the DLC film hardness will minimize the thickness of the DLC film and adherent layer, so that trade off between benefits.

A various strategies are used to maximize the DLC film thickness. First, it is essential to ensure there is a good adhesion between the film and the substrate. The film should fail by de-laminate between film and substrate. This can be obtaining by cleaning the surface by Ar ion bombardment prior deposition. Other method is to use high deposition ion energy for the first stage of deposition, to cause ion beam mixing between film and substrate in order to ensure that interfacial layer has been mixed.

Second, recently found that there is not certainly a direct correlation between stress and modulus [53], so that it may be possible to make low stress films with higher modulus.

Third, a carbide-forming adhesion layer such as Si, W and Cr can be deposited as seed layer prior the carbon deposition [54]. Si works well for glass substrate used in sunglasses and bar-code scanners, so that they have internal stress relief mechanisms.

Fourth, it is possible to use multi-layers to provide internal stress relief. This has been used by Meneve, et al. [55] for a-$CSi_x$:H films and by Anders, et al. [56] for ta-C films.

Finally, rather thick ta-C films have been formed by deposition on a soft intermediate layer of Al, Cu, Ti or AISI316 steel or similar with a Vickers hardness of less than 3 GPa [57-58]. The intermediate layer on top substrate, which could be Si. The idea is that the intermediate layer should yield locally below the film, and thereby absorb the effect of the compressive stress. Ion beam mixing is used for good adhesion to the soft substrate. The intermediate layer should be a carbide former (Ti, Fe, etc.) and if not a thin carbide forming layer such as Mo is used. It is also found that pulse cathodic arc give thicker films than continuously operating FCA in this case. It is able to deposit ta-C films well over 10 μm by this method.

The relaxation stress by alloying with for example Si [59-61] or metals [62-63] are a majority effort. Si has various beneficial effects. It can promote $sp^3$ bonding by chemical means, as it does not exert $sp^2$ hybridisation, so it is not necessary to use as much ion bombardment to get $sp^3$ bonding. It increases the thermal stability of the hydrogen. It also improves the friction performance, as discuss shortly, by maintaining a low friction to higher humidity. Si alloying is widely used to improve performance. Metals relax stress and also increase hardness and toughness, however, make the film opaque.

### 2.4.3 Wear

Wear is the removal of material during the contact process. Wear occurs by adhesion, abrasion or by corrosive/oxidative wear. For low applied loads, the load makes an elastic contact with the surface, and no permanent groove is left. There is no wear. At moderate loads, a permanent groove or wear track is left by plastic deformation or

abrasion. At high loads, a wear track of cracking and deformation remains. The wear is the volume of material removed from a surface by contact. The volume of wear per unit track length Q is given by

$$Q = KA \tag{2.3}$$

where A is the real contact area and is given as earlier by the ratio of load W to the pressure or hardness H of the soft surface, A = W / H . This gives the Archard equation,

$$Q = K\frac{W}{H} \tag{2.4}$$

where k is the wear coefficient, a dimensionless number. It is much less than 1. A dimensional wear coefficient k is often used, define by

$$Q = \frac{K}{H}W = kW \tag{2.5}$$

where k is usually given in unit of $mm^3\ N^{-1}m^{-1}$.

The Archard equation says that the wear coefficient is inversely proportional to the hardness of the surface. Hence harder surface wear less, and the aim for protective coating is to maximize their hardness. Gangopadhyay [49] have compared various types of DLC with other coating materials. These are are summarized in Table 2. It is found that ta-C has an extremely low wear rate of order $10^{-9}$ $mm^3\ N^{-1}m^{-1}$, this about a 100 times lower than that of a-C:H at $10^{-7}$ $mm^3\ N^{-1}m^{-1}$. The value for ta-C is impressively low. It is the low wear rate of ta-C which fundamentally make ta-C so suitable for MEMs devices.

**Table 2.2** Comparison of wear rate for ta-C and a-C:H.

| Wear rate ($mm^3\ N^{-1}\ m^{-1}$) | |
|---|---|
| ta-C | $10^{-9}$ |
| a-C:H | $10^{-6}$ to $10^{7}$ |

The wear mechanism of ta-C and a-C:H are the friction mechanism, adhesive wear via transfer layers. The ta-C transforms by stress induced transformation to a graphitic over-layer, which then acts as a lubricant, whereas a-C:H forms a C:H transfer later on the counter surface. The more $sp^2$ bonded a-C was found to wear by oxidation to $CO_2$ in an air ambient.

A novel form of carbon is hard carbon with fullerene-like inclusions. This is preparing by deposition on cathodic arc in the presence of nitrogen gas, or by sputtering carbon in a nitrogen atmosphere both at elevated temperature (~200 C). The local atomic structure has been view by high resolution transmission electron microscopy and EELS. The films show unusual mechanical properties of high hardness and very high elastic recovery. This could make them valuable for coating.

Nano-crystalline diamond is also much smoother than polycrystalline diamond, and it probably has superior friction and wear properties compared to DLC. However, it does require higher deposition temperatures.

### 2.4.4 Surface Property

DLC is also notable for it small surface energy [62]. The surface usually measured using the contact angle. The contact angle θ of a liquid on a DLC surface depends on the three energies, the surface energy of the DLC $\gamma_{sl}$, via the Young's equation,

$$\gamma_s = \gamma_{s1} + \gamma_1 \cos\theta \tag{2.6}$$

The surface energy is extracted by measuring θ for more than one liquid, and apportioning the tension between dispersive and dipole components. Low surface energies give large contact angles. Surface energies are typically 40-44 $mNm^{-1}$. The a-C:H generally has a contact angle with water of 55-70°. Unusually, this is found to be independent of deposition bias voltage.

The ta-C is also hydrophobic. Its contact angle of water lies in the range 75-80°. However, this is less than a-C:F. The addition of metal such as l and Fe reduces the surface energy to 25 $mNm^{-1}$ and make a-C more hydrophobic.

### 2.4.5 Optical Property

The optical spectra of amorphous carbon provide valuable information on their local electronic structure. The complex dielectric function is define in term of its real and imaginary parts as follow:

$$\varepsilon = \varepsilon_1 + i\varepsilon_2 \tag{2.7}$$

$\varepsilon_1$ and $\varepsilon_2$ are then given by

$$\varepsilon_1 = n^2 - k^2 \tag{2.8}$$

and

$$\varepsilon_2 = 2nk \tag{2.9}$$

Where n is the refractive index, k the extinction coefficient, $k = \propto / 4\pi\lambda$, where $\propto$ is the optical absorption coefficient and λ the wavelength. The variables $\varepsilon_1$ and $\varepsilon_2$ are related by the Kramers-Kronig relationship

$$\varepsilon_1(E) = 1 + \frac{1}{\pi}\int_0^\infty \frac{\varepsilon_2(E')dE'}{E - E'} \tag{2.10}$$

and is given by

$$\varepsilon_2(E) = \frac{(2\pi e^2)^2}{N}\int_0^\infty R^2(E) N_v(E') N_c(E + E')dE' \tag{2.11}$$

where N is the atomic density, R(E) is the distance dipole matrix element, and $N_v$ and $N_c$ are the valence and conduction band DOS, respectively. R(E) is generally reasonably independent of energy E.

The optical spectra for most materials are acquired by direct transmission-reflectivity experiments. In Si, the main bonding-antibonding transitions give rise to the $E_2$ peak at around 4.2 eV. The peak falls to 3.3 eV in a-Si due to the loss of the k-selection rule. The spectra features fall in the accessible 1-5 eV energy range of transmission-reflectivity measurements. However, carbon is unusual in that its strong bonds cause its spectra to span a much higher energy range than usual, 2-25 eV, and the important features lie above 5 eV. This means that the spectra must be measure on vacuum UV or energy loss systems.

## 2.5 Application in Hard Disk Drive (HDD)

One of the most important uses of DLC films is as protective coating on magnetic storage disks [50-51]. Magnetic storage is the most economic form of nonvolatile storage for many applications. Its great advantage is that the storage density is increasing at a very rapid rate [51]. Recently, storage densities are increasing at 40% per year.

Data are stored in a magnetic layer of Co–Cr–Pt alloy thin film. A protective layer of diamond-like carbon (DLC) coating is applied over the Co layer, and 1-2 monolayers of a perfluoro-polyether such as ZDOL or Fomblin is used as a molecular lubricant. A read/ write head flies above the rotating disk on an aerodynamic bearing. The read/write head consists of many layers of thin films and is also protected by a DLC film, Figure 2.21 and Figure 2.22 DLC films are used as coatings because they are extremely smooth, continuous and chemically inert, with surface roughness well below 1 nm.

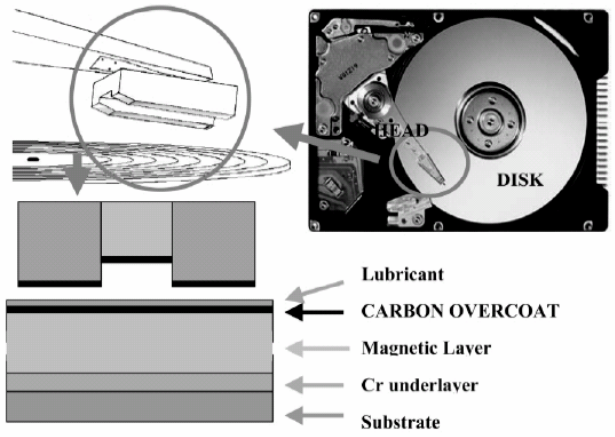


**Figure 2.21** Hard disk architecture.

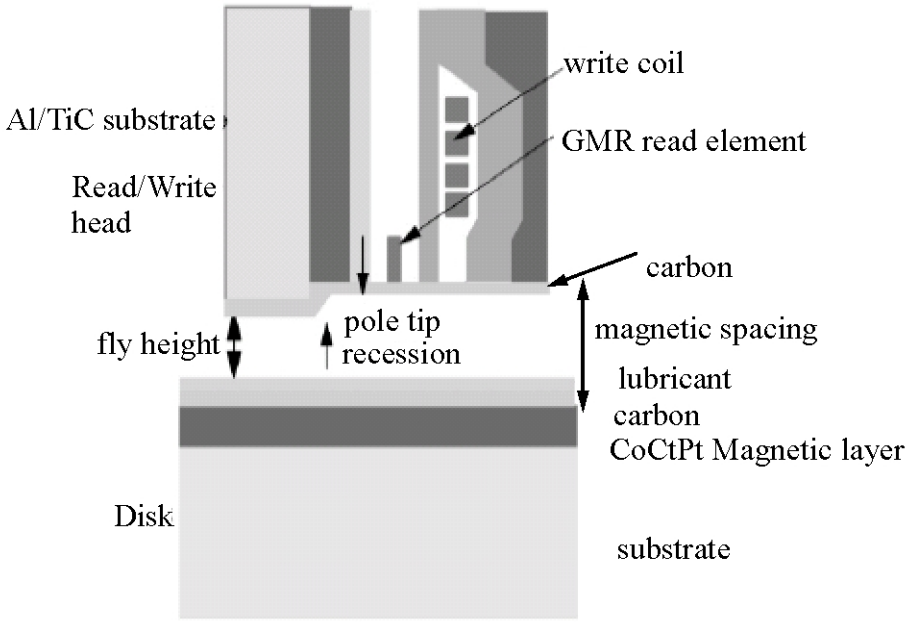


**Figure 2.22** Cross-section of head and disk interface.

The storage density is increased by reducing the area occupied by each bit of data. The areal density is the product of the tracks per inch and the bits per inch along a track. A smaller bit size requires a smaller magnetic spacing, which is the vertical distance between the read head and the Co storage layer (Figure 2.22). The magnetic spacing is slightly greater than the fly height, which is the separation of head and disk. Reducing the fly height requires ever-thinner carbon films. They are presently approximately 1-2 nm thick, as shown in Figure 2.23.

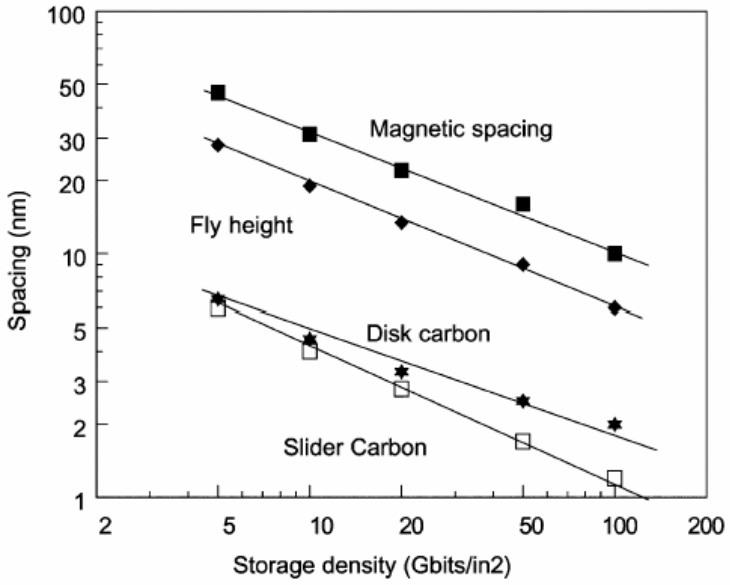


**Figure 2.23** Variation of carbon thickness on disk and slider, magnetic spacing and fly height with storage density.

DLC has been deposited by sputtering. Now, there is a transition, as the industry moves to new processes such as cathodic arc or plasma deposition needed to make the thinner films. The main role of such ultra-thin films is to provide a corrosion barrier to the recording medium. They must be atomically smooth, dense, continuous and pin-hole free. However, both a-C:N and a-C:H cease to provide protection against corrosion and wear below 3–4 nm thickness since magnetron sputtering is not able to make continuous and ultra-thin films. Highly $sp^3$ hydrogen-free DLC, tetrahedral amorphous carbon (ta-C), is now the preferred means of coating read heads, because of its unique combination of desirable properties, such as high hardness and wear resistance and chemical inertness to both acids and alkalis and atomic smoothness.

## 2.6 Characterization

### 2.6.1 Film Thickness

Thickness of a film is among the first quoted attributes of its nature. The reason is that-film properties usually depend on thickness. Historically the use of films in optical applications spurred the development of techniques capable of measuring film thicknesses with high accuracy. The actual film thickness, within broad limits, is particularly crucial to function in some application especially DLC and microelectronic coated applications generally require the maintenance of precise and reproducible film metrology, i.e., thickness as well as lateral dimension. Even more stringent thickness requirements must be adhered to in multilayer optical-coating applications.

### 2.6.2 Film Structure

There are several hierarchies of structural information which are of interest to thin-film scientists and technologists in research, process development, and reliability and failure analysis activities. These are listed next in roughly ascending order of structural resolution required. First broadly deals with metrology of patterned films where issues of lateral or depth dimensions and tolerance, uniformity of thickness and coverage, completeness of etching, etc., are of concern. Secondly, film surface topography and microstructure in plan view including grain size and shape, existence of compounds, presence of hillocks or wiskers, evidence of film voids, micro-cracking or lack of adhesion, etc., are of interest. Third are cross-sectional views of multilayer structures exposing interfacial regions, columnar grain morphology, and substrate interactions. Such images are crucial in microelectronics and optical coating technologies, enabling direct verification of device dimensions and structural defects in devices. Forth somewhat more challenging is the high-resolution lattice image of both plan-view and transverse film sections. Among the applications here are defect structure in films and devices, structure of grain boundaries, identification of phases, and a host of issues related to epitaxial structures, e.g., the crystallographic orientations, direct imaging of atoms at interface, interfacial quality and defects, and perfection of assorted thin film super lattices. Finally, there is structural information required of substrate and film surface such as the details of film-nucleation and growth processes, crystallography of deposits, and reconstruction of surface layers.

### 2.6.3 Chemical Composition

The chemical characterization of thin film includes identification of surface and near-surface atoms and compounds, as well as their lateral, depth spatial distributions and bonding structure. The chemical structure and properties of amorphous carbon coating are a function of deposition condition. It is important to understand the relationship of the chemical structure of amorphous carbon coating to the properties in order to define useful deposition parameters. Amorphous carbon films are metastable phases formed when carbon particles are condensed on a substrate. The prevailing atomic arrangement in the DLC coating is amorphous or quasi amorphous with small diamond ($sp^3$), graphite ($sp^2$), and other unidentifiable micro or nanocrystallities. The coating dependent upon the deposition process and its conditions contain varying amounts of $sp^3$/ $sp^2$ ratio and H. The $sp^3$/$sp^2$ ratio of DLC coatings ranges typically from 50% to 100% with an increase in hardness with $sp^3$/ $sp^2$ ratio.

## 2.7 Metrology of DLC Film

### 2.7.1 Thickness Measurement

Basically can be divided into mechanical and optical, and are usually nondestructive but sometime destructive in nature

#### 2.7.1.1 Transmission Electron Microscopy (TEM)

The transmission electron microscope (TEM) is electron analogue of the optical compound microscope. As a gross simplification, the TEM may be compare to slide projector with the slide (specimen) illuminated by light (electron beam) that first passes through the condenser lens (electromagnetic condenser lens). The transmitted light from an image that is magnified by the projector lens (electromagnetic objective and projector lenses) and view on screen (or photographed). In operation, electrons are thermionically emitted from the gun and typically accelerated to anywhere from 125 to 300 keV, or higher in some microscopes. High magnification in TEM method is a result of the small effective wavelength (λ) employed. According to the deBroglie relationship.

$$\lambda = \frac{h}{(2mqV)^{1/2}} \tag{2.12}$$

Where m and q are the electron mass and charge, and V is the potential difference. Electron of 100 keV energy have wavelengths of 0.037 Å and are capable of effectively transmitting through about 0.6 μm of Si. In operation, electrons are projected onto the specimen by condenser lens system. The scattering processes they undergo during their passage through the specimen determine the kind of information obtained. Elastic scattering, involving no energy loss when electrons interact with the potential field of the ion cores, gives rise to diffraction patterns. Inelastic interactions between beam and matrix electrons at heterogeneities such as grain boundaries, dislocation, second-phase particles, defects, and density variations cause complex absorption and scattering effects leading to a spatial variation in the intensity of transmitted beam. Primary and diffracted

electron beams that emerge from the specimen are now made to pass through a series of post specimen lenses. The objective lens produces the first image of the object beams reaching the back focal plane of the objective lens are subsequently process distinguishes the difference methods of operation.

There are two very broad modes of TEM operation, namely imaging and analytical. In the former, structural images ranging from low magnification to atomic resolution are directly revealed, whereas in the latter structural information is indirectly revealed through analysis of diffracted beam geometries and energies. These modes are differentiated in Figure 2.24 (a) and (b), where the lenses, beam path, and method of image formation are schematically indicated. Each of techniques depicted is briefly described in turn below.

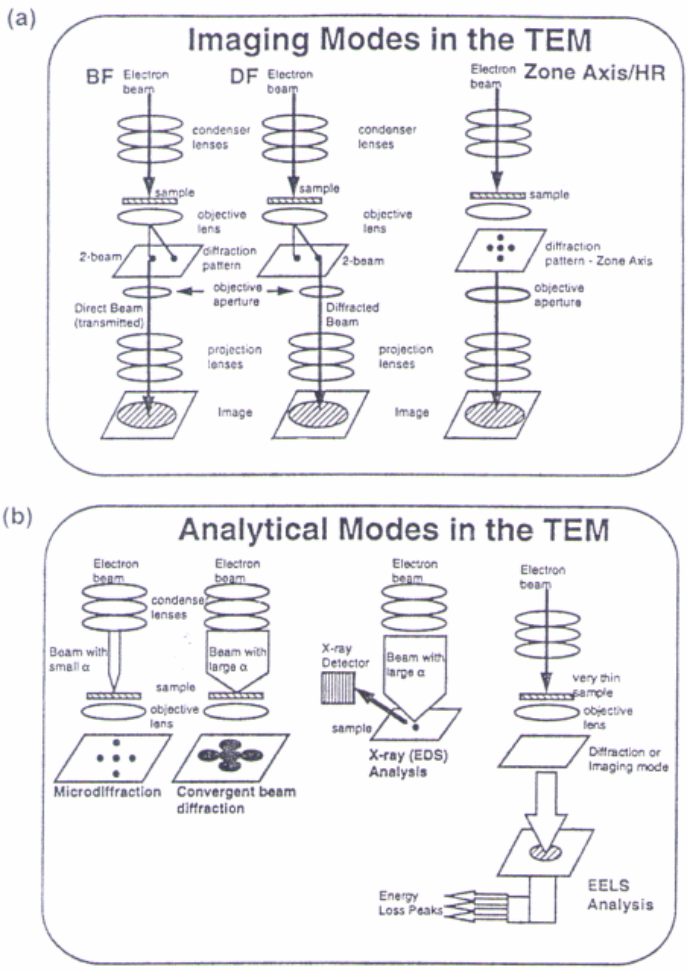


**Figure 2.24** Two modes of TEM operation, (a) imaging mode, (b) analytical mode.

(1) Bright-field imaging (BF). Also known as conventional TEM, bright-field imaging intentionally excludes all diffracted beams and only allows the central beam through. This is done by placing suitably sized apertures in the back focal plane of the subjective lens. Intermediate and projection lenses then magnify this central beam to provide images of the microstructure and morphology of features.

(2) Dark-field imaging (DF). Dark-field images are also formed by magnifying a single beam; this time one of the diffracted beams is chosen by mean of an aperture which blocks both the central beam and the other diffracted beams.
(3) Lattice imaging. In this now-popular method of imaging periodic structure with atomic resolution, the primary transmitted and one or more of the diffracted beam are made to recombine, thus preserving both beam amplitude and phases.
(4) Diffraction. Diffraction yields crystallographic and orientation effect information on structural features, defects, and phases.
(5) X-ray spectroscopy. This analytical capability, otherwise known as X-ray energy dispersive analysis (EDX), allows elemental identification through measurement of characteristic X-ray energies.
(6) Electron energy loss spectroscopy (EELS). Through energy analysis of particularly useful for detecting low-Z elements.

### 2.7.1.2 TEM Cross-Section

Perhaps the most dramatic image of film structure and devices are those taken in cross section. In this important technique, specimens that are already thin in one dimension are now thinned in the transverse direction; it is like imaging this page in edge view rather than in the plane the words appear on. What is involved in the case of integrated circuits is cleaving a number of wafer specimens transversely, bonding these slivers in an epoxy button, and thinning them by grinding and polishing. Finally, the resulting head is ion milled until a hole appears. By preparing many specimens simultaneously the probability of capturing images from desired device features is enhanced.

As an outstanding example of a TEM cross-sectional image, consider the DLC/a-Si films thickness as shown in Figure 2.25.

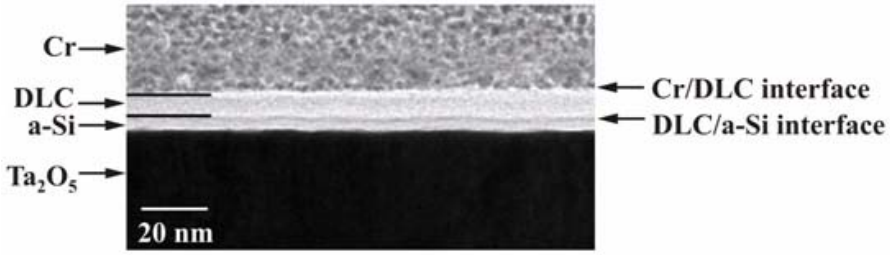


**Figure 2.25** A TEM cross-sectional view of a nano-field-effect transistor thinned by conventional methods (not FIB).

### 2.7.1.3 Focused Ion Beam Microscopy (FIB)

The use of focused ion beam (FIB) represents a recent major advance in TEM sample preparation as well as for microscopy in its own. Briefly, the FIB systems operate in a similar fashion to a scanning electron microscope (SEM) except, rather than a beam of electrons and as the name implies, FIB systems use a finely focused beam of ions (usually gallium) that can be operated at low beam currents for imaging or high beam currents for site specific sputtering or milling.

Figure 2.26 shows the diagram the principle of FIB, the gallium ($Ga^+$) primary ion beam hits the sample surface and sputters a small amount of material, which leaves the surface as either secondary ions ($i^+$ or $i^-$) or neutral atoms (n0). The primary beam also produces secondary electrons (e-). As the primary beam rasters on the sample surface, the signal from the sputtered ions or secondary electrons is collected to form an image.

At low primary beam currents, very little material is sputtered and modern FIB systems can easily achieve 5 nm imaging resolution (imaging resolution with Ga ions is limited to ~5 nm by sputtering [64-65] and detector efficiency). At higher primary currents, a great deal of material can be removed by sputtering, allowing precision milling of the specimen down to a sub micrometre scale.

If the sample is non-conductive, a low energy electron flood gun can be used to provide charge neutralization. In this manner, by imaging with positive secondary ions using the positive primary ion beam, even highly insulating samples may be imaged and milled without a conducting surface coating, as would be required in a SEM.

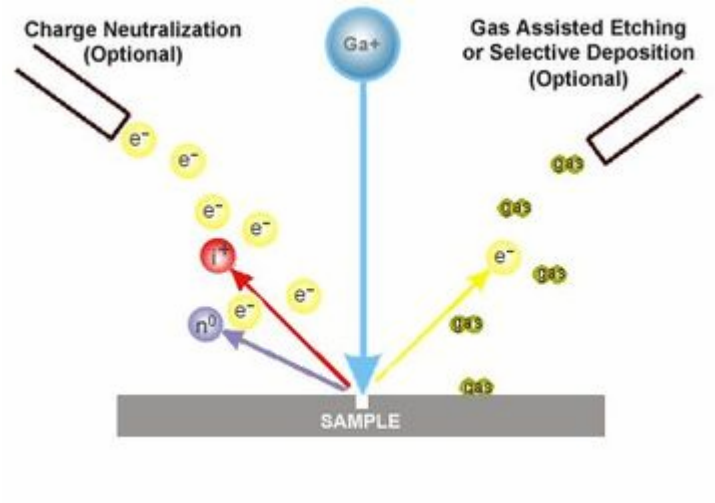


**Figure 2.26** Principle of FIB.

### 2.7.1.4 Spectroscopic Ellipsometry

Ellipsometric theory is based on Fresnel reflection or transmission equations for polarized light encountering boundaries in planar multi-layered materials [66-67], based on Maxwell's equations [68]. The ellipsometric measurement is normally expressed in terms of Psi (Ψ) and Delta (Δ):

$$\tan(\psi).e^{i\Delta} = \rho = \frac{r_p}{r_s} \tag{2.13}$$

where '$r_p$' and '$r_s$' are the complex Fresnel reflection coefficients of the sample for p- (in the plane of incidence) and s- (perpendicular to the plane of incidence) polarized light, illustrated in Figure 2.27. These coefficients contain desired information related to material optical properties and physical dimensions. Spectroscopic Ellipsometry (SE) measures this complex ratio as a function of wavelength (or photon energy) [69], they are sensitive to ultra-thin films (<1 nm).

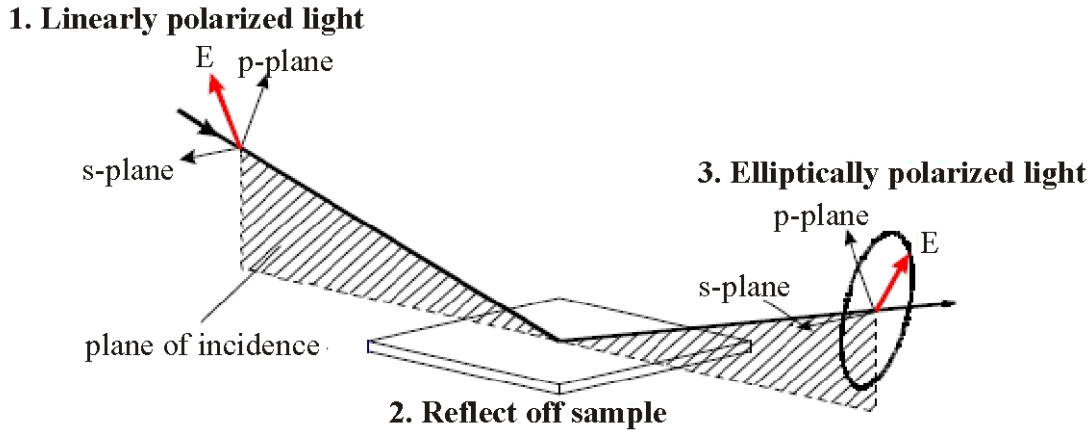


**Figure 2.27** Basic configuration for reflection ellipsometry.

Ellipsometry measures the change in polarization expressed as Ψ and Δ. To extract useful information about a material structure, it is necessary to perform a model dependent analysis of the ellipsometric data.

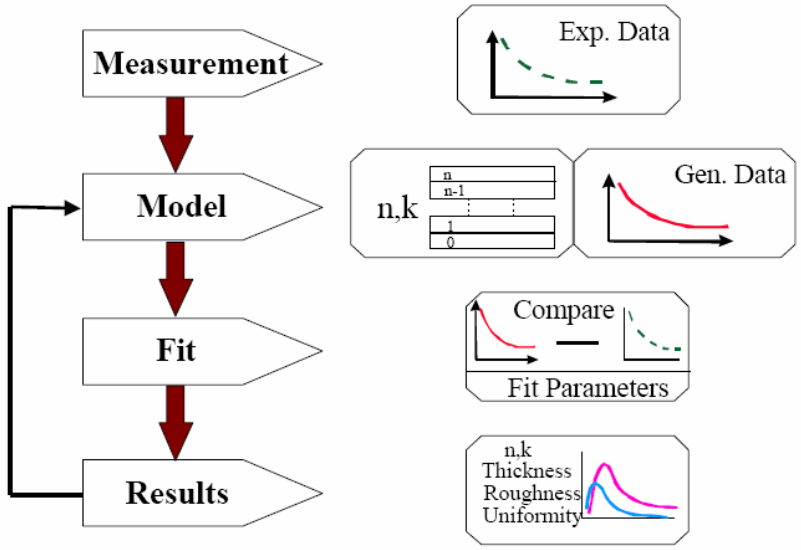


**Figure 2.28** Flowcharts for analysis procedure.

Figure 2.28 shows outline of this process. For a single-layer or a multi-layer sample, the measured SE data are acquired covering the desired spectral range and angles of incidence from it may be analyzed with an appropriate fitting model, which should best represent the structure of the sample under study. For example, this may include a substrate and a single film on the surface, or substrate plus film with roughness on top or more complex structures. In this model, unknown parameters, such as layer thickness and/or composition, can be used as fitting parameters to be determined from the standard ellipsometric equations [66-67]. With the help of a regression fitting algorithm [70-71], the measured spectra are fitted objectively by minimizing the squared differences between the measured and calculated Ψ and Δ values, which are generated

from the fitting model at the corresponding wavelengths and angle of incidence. In some cases, optical constants are available from published tables [72-75].

The most commonly used is the Marquardt-Levenberg algorithm [70-71]. The objective is to quickly determine the minimum difference or "best fit" between the measured and calculated Ψ and Δ values. The (Root) Mean Squared Error (MSE) quantifies this difference. A smaller MSE implies a better model fit to the data. The MSE can be normalized by the standard deviation to reduce the weighting of noisy data. The quality of the fit can be judged by the MSE function commonly used is given below [76].

$$MSE = \sqrt{\frac{1}{2N-M}\sum_{i=1}^{N}\left[\left(\frac{\Psi_i^{Mod}-\Psi_i^{Exp}}{\sigma_{\psi,i}^{Exp}}\right)^2+\left(\frac{\Delta_i^{Mod}-\Delta_i^{Exp}}{\sigma_{\Delta,i}^{Exp}}\right)^2\right]} \tag{2.14}$$

where N is the number of (Ψ and Δ) pairs, M is the number of variable parameters in the model, superscripts Mod and Exp represent the calculated and measured data, respectively, and σ are the standard deviations on the experimental data points. Regression analysis requires the correct model to achieve good fits to the experimental SE data. If the model does not adequately represent the true structure, then good matches between experiment and theory are not typically found, and the model needs to be reformulated.

The Tauc-Lorentz (TL) dispersion derived by Jellison and Modine, has been propose by integrating quantum mechanics with the classical spring-mass system, by combining the Tauc band edge with the classical Lorentz broadening function. The Tauc-Lorentz optical model, however, requires additional parameters, i.e., oscillator strength, peak transition energy, broadening function and energy gap. Which proposes an expression for the imaginary part of the dielectric function given by:

$$\varepsilon_2 = \frac{AE_0C(E-E_g)^2}{(E^2-E_0^2)^2+C^2E^2}.\frac{1}{E} \tag{2.15}$$

if $E > E_g$ and $\varepsilon_2 = 0$ if $E < E_g$. In this expression, $E_0$ is the peak transition energy, $C$ the broadening term and $A$ is related to the transition probability; $\varepsilon_1$ is calculated by the Kramers-Kroning dispersion relation, then $\varepsilon_1$ can be derived,

$$\varepsilon_1(E) = \varepsilon_1(\infty) + \frac{2}{\pi}p\int_{E_g}^{\infty}\frac{\xi\varepsilon_2(\xi)}{\xi^2-E^2}d\xi \tag{2.16}$$

Spectroscopic ellipsometry is quite sensitive to surface and interface structure. In some case, the optical constants of a material of interest can be adequately described by mixing the optical constants of two known materials. The mixture is done using the Bruggeman effective medium approximation (BEMA)) [77-78]. The BEMA is method of treating a macroscopically inhomogeneous medium where quantities, such as the conductivity σ, dielectric function ε, or elastic modulus vary in space. Accordingly, the effective dielectric function $\in_{eff}$ of the mixture was obtained from the following equations:

$$\sum_i f_i \left[ (\in_i - \in_{eff}) / (\in_i + 2 \in_{eff}) \right] = 0 \tag{2.17}$$

and

$$\sum_i f_i = 1 \tag{2.18}$$

where $f_i$ and $\in_i$ are the volume fraction and the dielectric function of the ith constituent material in the mixture, respectively.

## 2.7.2 Surface Morphology

### 2.7.2.1 Atomic Force Microscopy (AFM)

The AFM consists of a cantilever with a sharp tip (probe) at its end that is used to scan the specimen surface. The cantilever is typically silicon or silicon nitride with a tip radius of curvature on the order of nanometers. When the tip is brought into proximity of a sample surface, forces between the tip and the sample lead to a deflection of the cantilever according to Hooke's law. Depending on the situation, forces that are measured in AFM include mechanical contact force, van der Waals forces, capillary forces, chemical bonding, electrostatic forces, magnetic forces (see magnetic force microscope, MFM), Casimir forces, solvation forces, etc. Along with force, additional quantities may simultaneously be measured through the use of specialized types of probe (see scanning thermal microscopy, scanning joule expansion microscopy, photothermal microspectroscopy, etc.). Typically, the deflection is measured using a laser spot reflected from the top surface of the cantilever into an array of photodiodes. Other methods that are used include optical interferometry, capacitive sensing or piezoresistive AFM cantilevers. These cantilevers are fabricated with piezoresistive elements that act as a strain gauge. Using a Wheatstone bridge, strain in the AFM cantilever due to deflection can be measured, but this method is not as sensitive as laser deflection or interferometry. The AFM schematic diagram as shown in Figure 2.29.

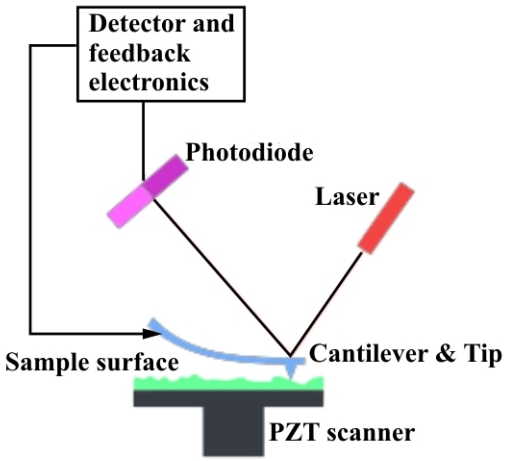


**Figure 2.29** Block diagram of atomic force microscope.

### 2.7.3 Chemical Bonding Structure

#### 2.7.3.1 Bonding Structure Characterization

Raman spectroscopy is the best way to obtain the detail of bonding structure of DLC due to it is fast and non-destructive way to characterization the structure quality of diamond, graphite, nanotubes [79] and DLC. Diamond has a single Raman active mode at 1332 $cm^{-1}$, which is the zone-centre mode of $T_{2g}$ symmetry. Single crystal graphite has a single Raman active mode, which is the zone-centre mode at 1580 $cm^{-1}$ of $E_{2g}$ symmetry labeled 'G' for 'graphite'. Disordered graphite has a second mode at around 1,350 $cm^{-1}$ of $A_{1g}$ symmetry labeled 'D' for 'disorder for visible excitation. At the 514 nm excitation. Raman spectra of most disordered carbon remain dominated by these two G and D modes of graphite, the $sp^2$ sites have such a high cross-section that they dominate the spectra, the $sp^3$ sites are invisible and the spectrum responds only to the configuration or order of the $sp^2$ sites. So the G and D peaks are due to $sp^2$ sites. The G peak is due to the bond stretching of all pairs of $sp^2$ atoms in both ring and chains. The D peak is due to the breathing mode of $sp^2$ atoms in ring as shown in Figure 2.30.

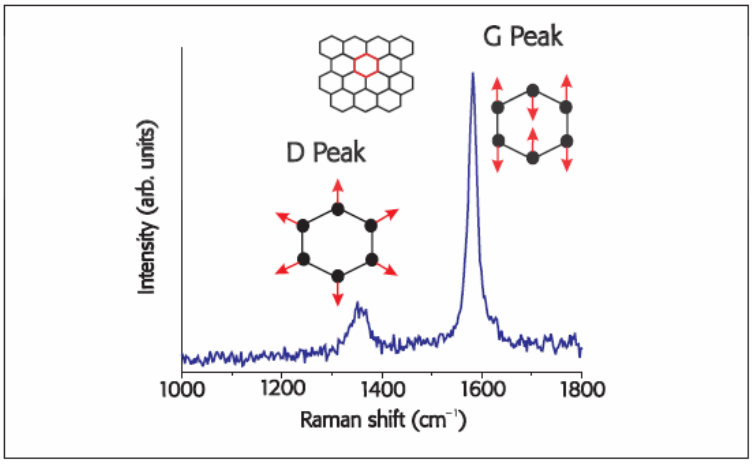


**Figure 2.30** 514 nm Raman spectrum of highly orientated graphite.

Figure 2.31 shows the typical DLC Raman spectra (red line) between 1130 and 1800 $cm^{-1}$. Further analysis of Raman spectra were made by fitted to two peaks using a mixture of Gaussian and Lorentzian profiles, in order to analyze the spectra quantitatively; the Raman spectra were fitted using Gaussian profile (black line). A typical fitted spectra of DLC, the spectra can be fitted with two Gaussian-Lorentzian functions. Consequently, two broad peaks, G and D, centered approximately at 1570 and 1350 $cm^{-1}$, respectively were obtained as shown in Figure 2.32.

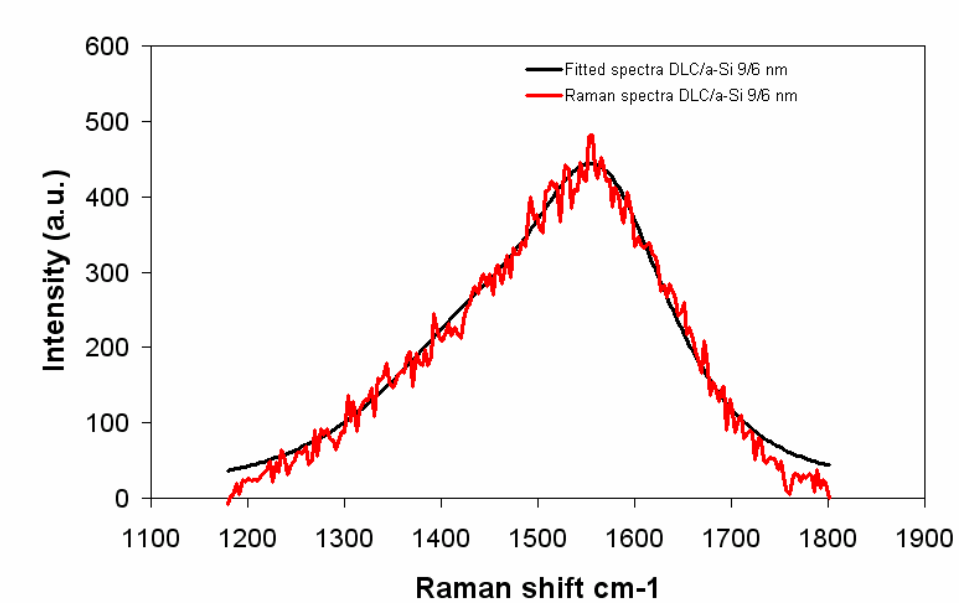


**Figure 2.31** Showing raw Raman spectra and fitted spectra of DLC.

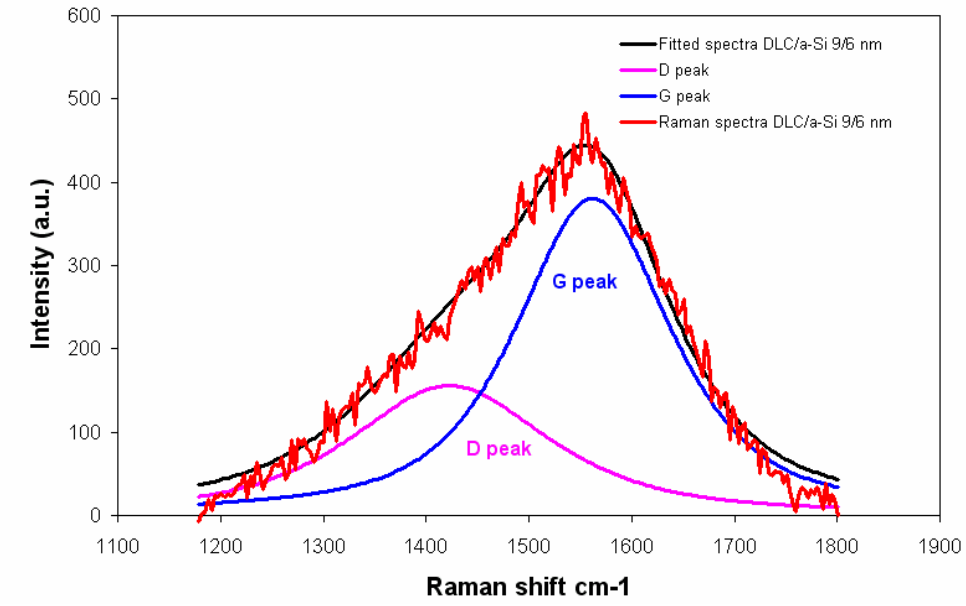


**Figure 2.32** Raman spectra were fitted into two peaks of DLC.

Raman excited by visible photons at 514 or 488 nm is only sensitive to the $sp^2$ site, because of their much greater cross-section than $sp^3$ sites. This is because visible light energy does not higher than lying σ states. UV Raman at 244 nm (5.1 eV) can be provides an excitation of σ states both $sp^3$ and $sp^2$ sites. So that it is directly observed $sp^3$ sites.

Figure 2.33 shows comparison the Raman spectra of ta-C film with various excitation wavelengths. A new peak labeled T has appeared at 1050-1100 $cm^{-1}$. This wavenumber is close to the expected maximum of vibration density of state of a fully $sp^3$ bonded random network.

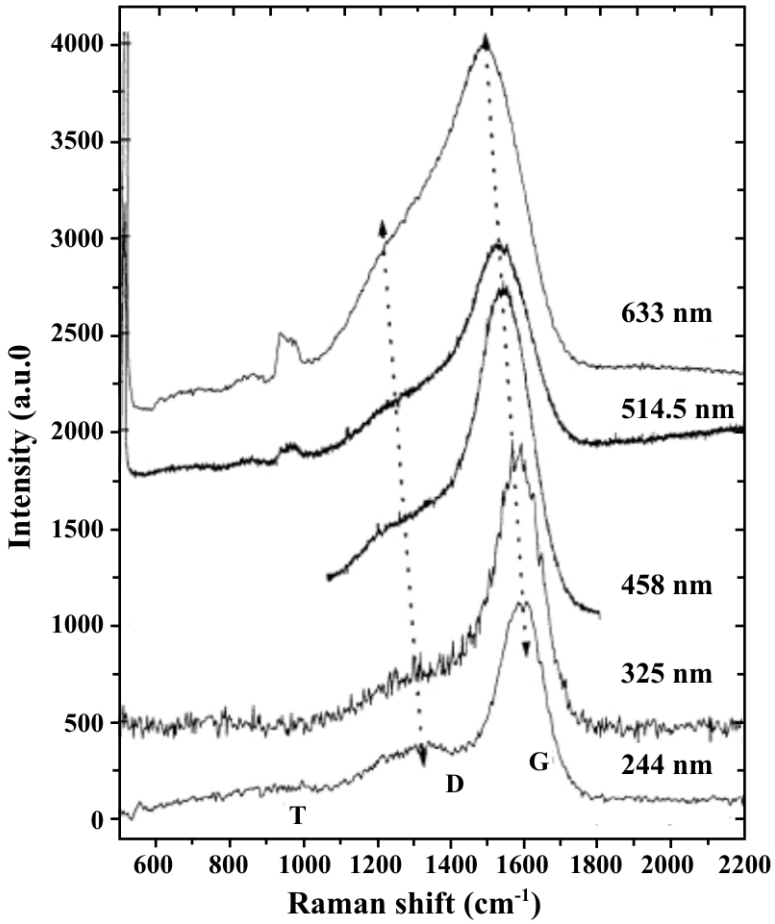


**Figure 2.33** Raman spectra with various excitation wavelengths for ta-C.

### 2.7.3.2 X-ray Photoelectron Spectroscopy (XPS)

X-ray photoelectron spectroscopy (XPS) is a surface chemical analysis technique with the capability of determining elemental composition, oxidation state, empirical formula and impurities present in a sample. XPS takes advantage of the photoelectric effect: it measures the kinetic energy of electrons that are ejected from a sample after irradiation by x-rays. The kinetic energy of an ejected electron is related to the binding energy of that electron for a certain atom. In this way, binding energies can be used to assign peaks to atoms in a typical spectrum, the XPS block diagram as shown in Figure 2.34.

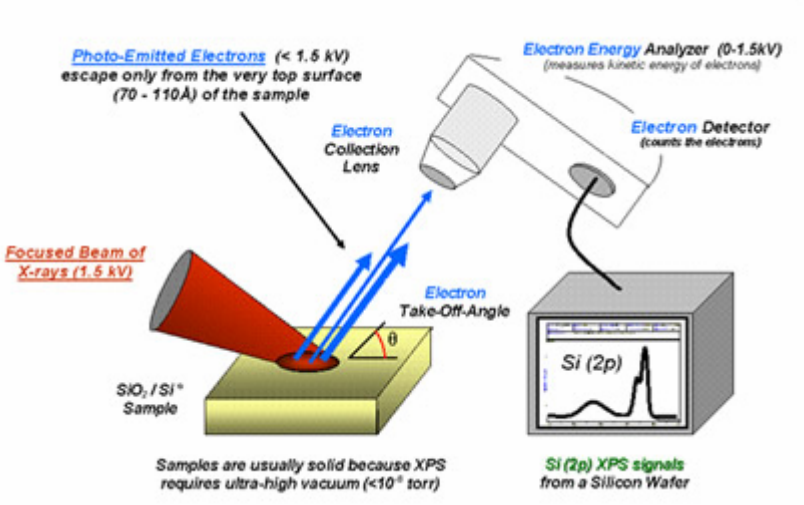


**Figure 2.34** Block diagram of X-ray photoelectron spectroscopy.

**Depth profile mode;** One of the increased capabilities is the depth profiling function which allows quantified elemental information with depth to be gathered. Figure 2.35 shows an ion beam is used to slowly etch away the surface revealing subsurface information which can then be analyzed Depths profile of elements from the outer surface through substrate. XPS depth profiling has been utilized to determine the layer thickness of coatings as well as characterizing multi-layer coatings.

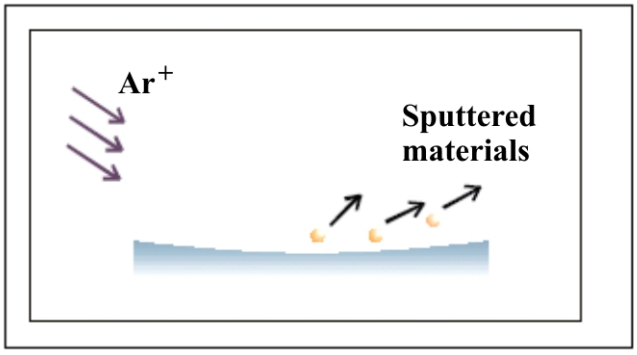


**Figure 2.35** $Ar^+$ ion sputtering of the outer surface.

Typical a commercially available, a depth profile can be seen measurements are taken as the ion beam etches through the material, profiling with the results shown in the Figure 2.36.

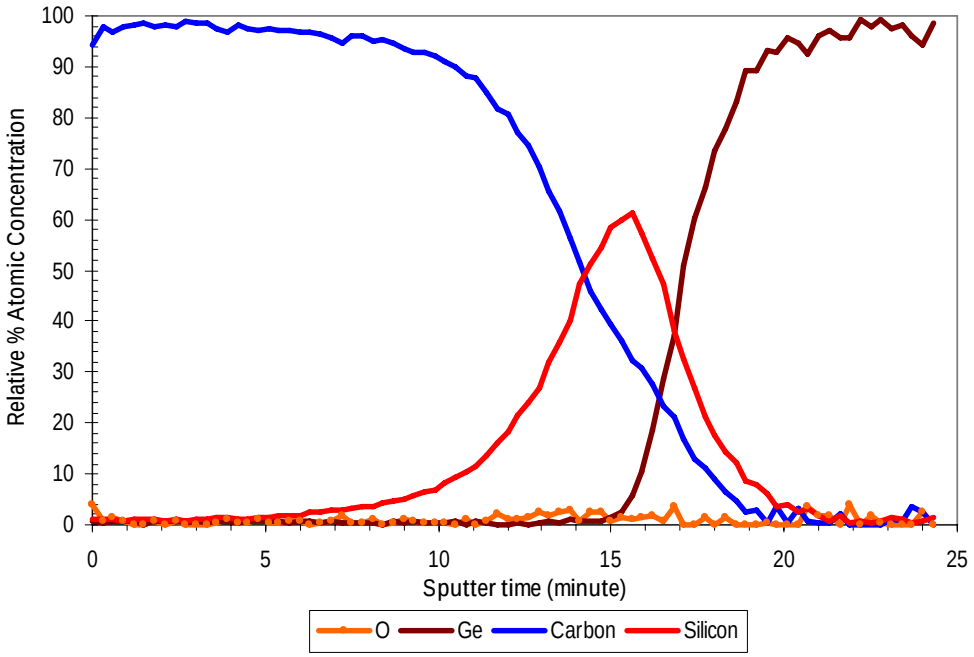


**Figure 2.36** XPS depth profile.

Three distinct layers can be seen on the profile. Layer 1 0 to 14 minutes is protective layer containing carbon. Layer 2 13 to17.5 minutes is seed layer containing silicon. Layer 3 above 17 minutes is the germanium substrate. Also the intersection times between layers existing are interfacial layer. (Note; thickness can be converse to nm unit by known etch rate sensitivity of each element)

### 2.7.4 Mechanical Property Measurement

Diamond-like carbon is a very important material for anti-wear films in the semiconductor and computer industry. Film thicknesses are typically on the order of 10 nm. In this case, substrate effects are almost impossible to avoid during indentation testing.

#### 2.7.4.1 Wear Measurement

Scanning wear testing is the process of creating a worn region by applying loads that generate friction for removal or movement of material. By applying higher loads and reducing scan size, wearing of material will occur. Imaging of this worn region is accomplished by increasing the scan size larger than the worn region and scanned at lower force, 1 µN to 1.5 µN. Figure 2.37 shows worn out region after applied load 40 µN with scan 2 passed. The average depth was around 14 nm as shown Figure 2.38.

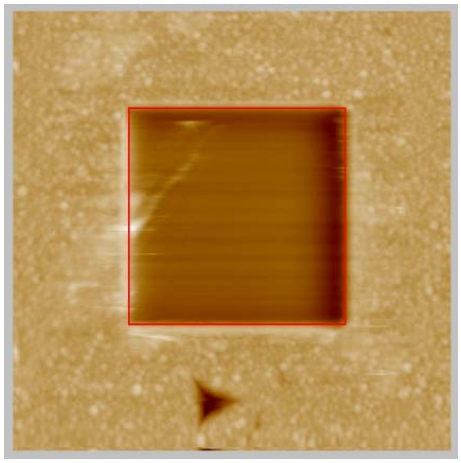

**Figure 2.37** Worn out region at load 40 µN with scanning of 2 passes.

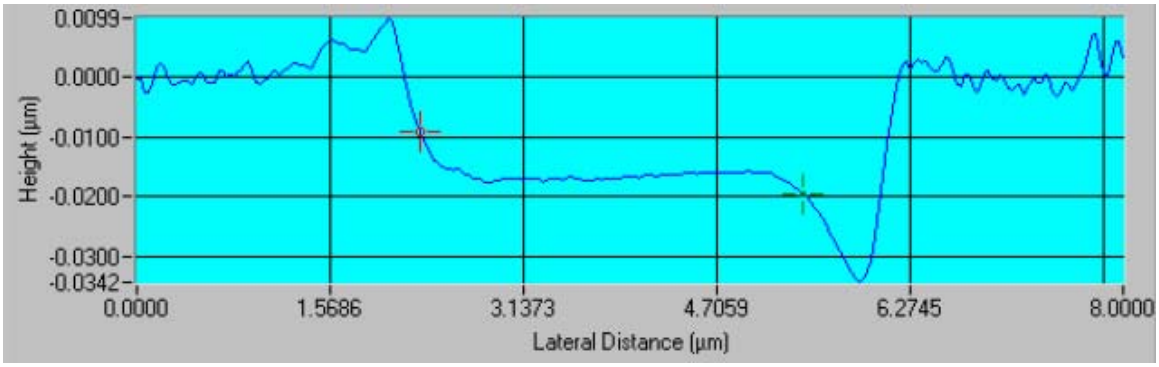


**Figure 2.38** Worn out region average depth [80].

### 2.7.4.2 Scratch Measurement

Scratch testing of DLC films is a useful alternative to evaluate adhesion and mechanical properties. Figure 2.39 shows a ramped load scratches 3 µm in length were made with a ramped normal force from 0 to 50µN on a 1 um DLC film on single crystal silicon (100) substrates using cathodic arc deposition. Figure 2.40 shows scratched testing, the critical load needed to penetrate 10nm DLC films and initiate film failure with a sharp cube corner tip was 38 ±2.8µN [81].

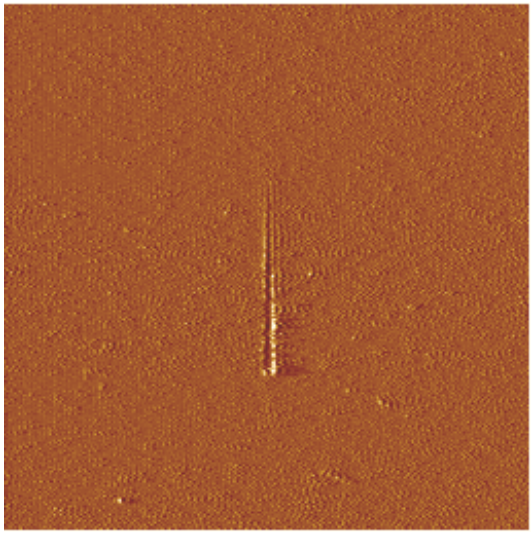

**Figure 2.39** Residual impressions from a scratch test in a 1 um DLC film using ramped force up to 50 μN.

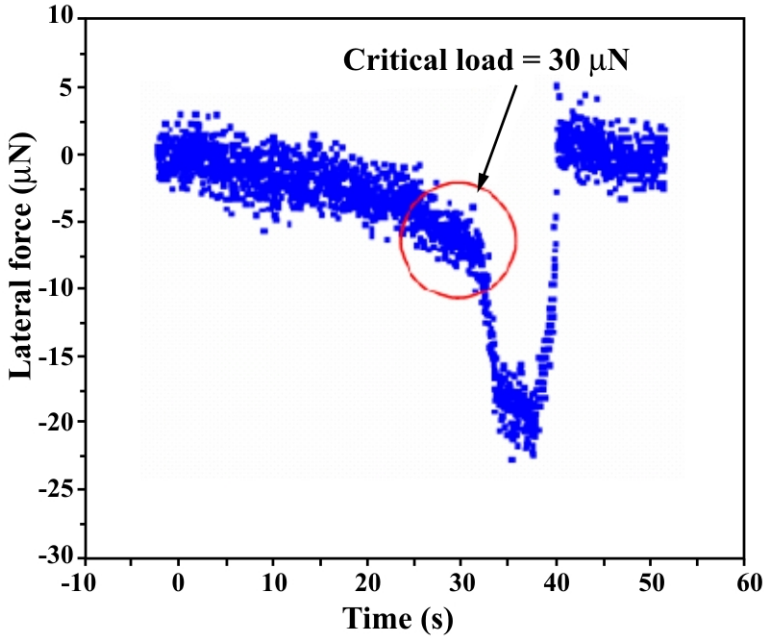


**Figure 2.40** Plot showing drop in lateral force during scratch measurement indicating film failure at 38 μN load [81].